Effects of amorphous silica coating on cerium oxide nanoparticles induced pulmonary responses

CrossMark

Jane Ma [a,*], Robert R. Mercer [a], Mark Barger [a], Diane Schwegler-Berry [a], Joel M. Cohen [b], Philip Demokritou [b], Vincent Castranova [c]

[a] Health Effects Laboratory Division, National Institute for Occupational Safety and Health, Morgantown, WV, USA
[b] Harvard TH Chan School of Public Health, Harvard University, Boston, MA, USA
[c] School of Pharmacy, West Virginia University, Morgantown, WV, USA

ABSTRACT

Recently cerium compounds have been used in a variety of consumer products, including diesel fuel additives, to increase fuel combustion efficiency and decrease diesel soot emissions. However, cerium oxide (CeO_2) nanoparticles have been detected in the exhaust, which raises a health concern. Previous studies have shown that exposure of rats to nanoscale CeO_2 by intratracheal instillation (IT) induces sustained pulmonary inflammation and fibrosis. In the present study, male Sprague–Dawley rats were exposed to CeO_2 or CeO_2 coated with a nano layer of amorphous SiO_2 ($aSiO_2/CeO_2$) by a single IT and sacrificed at various times post-exposure to assess potential protective effects of the $aSiO_2$ coating. The first acellular bronchoalveolar lavage (BAL) fluid and BAL cells were collected and analyzed from all exposed animals. At the low dose (0.15 mg/kg), CeO_2 but not $aSiO_2/CeO_2$ exposure induced inflammation. However, at the higher doses, both particles induced a dose-related inflammation, cytotoxicity, inflammatory cytokines, matrix metalloproteinase (MMP)-9, and tissue inhibitor of MMP at 1 day post-exposure. Morphological analysis of lung showed an increased inflammation, surfactant and collagen fibers after CeO_2 (high dose at 3.5 mg/kg) treatment at 28 days post-exposure. $aSiO_2$ coating significantly reduced CeO_2-induced inflammatory responses in the airspace and appeared to attenuate phospholipidosis and fibrosis. Energy dispersive X-ray spectroscopy analysis showed Ce and phosphorous (P) in all particle-exposed lungs, whereas Si was only detected in $aSiO_2/CeO_2$-exposed lungs up to 3 days after exposure, suggesting that $aSiO_2$ dissolved off the CeO_2 core, and some of the CeO_2 was transformed to $CePO_4$ with time. These results demonstrate that $aSiO_2$ coating reduce CeO_2-induced inflammation, phospholipidosis and fibrosis.

Published by Elsevier Inc.

1. Introduction

Cerium, a lanthanide member of the rare earth (RE) metals, has a variety of industrial applications and recently has been used as diesel fuel additive in conjunction with a particulate filter to reduce the ignition temperature of the carbonaceous diesel exhaust particles (DEPs). This results in more efficient burning of DEP and the regeneration of the particulate filter (HEI, 2001; Prospect, 2009). Using cerium as a catalyst substantially decreases both particle mass (>90%) and number (99%) in the diesel exhaust; however, a small amount of cerium oxide (CeO_2) nanoparticles is emitted in the particulate phase of the exhaust (HEI, 2001). Other studies further demonstrated that cerium was generated in the diesel exhaust from an engine using standard diesel fuel spiked with either CeO_2 or suspension of "Envirox", a commercial diesel fuel combustion catalyst based on CeO_2 (Cassee et al., 2012).

Animal studies have demonstrated that exposure of rats to nano scale CeO_2 by intratracheal instillation induced persistent lung inflammation and injury throughout a 28 day post-exposure period with the retention of particles in the exposed lungs (Ma et al., 2011; Molina et al., 2014). Other studies have shown that intratracheal exposure of CeO_2 induced pulmonary inflammation and small granulomas in both rats (Toya et al., 2010) and mice (Park et al., 2010), and that exposure of mice to CeO_2 through head and nose inhalation caused chronic inflammatory responses (Srinivas et al., 2011). Our previous studies have demonstrated that CeO_2 exposure induced pulmonary phospholipidosis, activated alveolar macrophage (AM) production of inflammatory cytokines, and induced fibrogenic and extracellular membrane (ECM) mediator production leading to pulmonary fibrosis (Ma et al., 2012).

Pulmonary fibrosis is characterized by an excessive deposition of extracellular matrix in the interstitium, where fibroblasts play a major role in the reconstruction of damaged connective tissue by producing new ECM components. The balance between ECM synthesis and degradation of matrix components is crucial for tissue repair, a process that requires a balance between matrix metalloproteinases (MMPs), which represent

a family of extracellular and cell surface-associated proteinases, and tissue inhibitors of matrix metalloproteinases (TIMPs). Abnormal activation of proteolytic and/or antiproteolytic functions can lead to lung diseases, including fibrosis (Gueders et al., 2006). Indeed, in human idiopathic pulmonary fibrosis (IPF), ECM accumulation with upregulated fibroblast proliferation has been demonstrated to result from excessively elevated TIMPs compared to MMPs, leading to a non-degrading fibrillar collagen microenvironment (Selman et al., 2000).

Diesel exhaust exposure alone induces adverse cardiopulmonary effects. The use of cerium as fuel catalyst leads to altered emission characteristics and induced more adverse pulmonary effects than DEP (Ma et al., 2014; Snow et al., 2014). The suggested effects of the combination of DEP and CeO_2, thus, raises concerns of health effects due to the presence of CeO_2 in diesel exhaust. The translocation of CeO_2 from the lung to other organs via circulation has also been demonstrated in the CeO_2-exposed animals (He et al., 2010; Ma et al., 2014; Molina et al., 2014; Nalabotu et al., 2011). These studies demonstrate that nano-ceria could penetrate through the alveolar wall into the systemic circulation and accumulate in the extrapulmonary organs, including lymph nodes and liver, leading to more adverse health concerns when using cerium as a diesel fuel catalyst.

It has been reported in a rat model that nearly 80% of the instilled CeO_2 was deposited in the lung at 24 h post-instillation. In addition, ~64% of the given CeO_2 remained in the lung 28 days after exposure, with an elimination half-life of 103 days (He et al., 2010). In vitro studies revealed minimal translocation (<0.1%) of CeO_2 across alveolar epithelial monolayers via trans- and para-cellular pathways (Cohen et al., 2014). Tissue distribution studies demonstrated that CeO_2 particles were detected in AM, mixed with accumulated lung surfactant in the alveolar air space, and in the alveolar interstitial tissue at 28 days post-exposure (Ma et al., 2011). Semmler-Behnke et al. (2007) proposed a long-term nanoparticle clearance mechanism, involving AM-mediated translocation of particles to the interstitial lymphatics and removal towards the larynx with subsequent re-entrainment into the airway lumen. Considering the long elimination half-life and the ceria/cerium-related pathogenesis of pneumoconiosis (McDonald et al., 1995; Porru et al., 2001; Sabbioni et al., 1982), exposure to the increased CeO_2 in diesel exhaust and from CeO_2 enabled products has raised health concerns. Recently, a "safer by design" concept for reducing the CeO_2-mediated toxicity has been pursued. A concept is based on encapsulation of flame generated nanoparticles with a nanothin amorphous silica (aSiO_2) layer during their synthesis in aerosol reactors, as reported by Gass et al. (2013). Based on this concept, nanoparticles of CeO_2 and aSiO_2-nanothin coated CeO_2 (aSiO_2/CeO_2) aerosols were generated by the Harvard Versatile Engineered Nanomaterial Generating System (VENGES) directly connected to a whole-body animal inhalation chamber, and the pulmonary inflammatory responses were monitored (Demokritou et al., 2012). The most important feature of VENGES is that the freshly generated particles of nano size directly entered the animal exposure chamber, while the commonly used aerosol generators, which disperse nanopowders, produce aged, agglomerated particles (Fischer and Chan, 2007; Schmoll et al., 2009). Based on this design, our studies have demonstrated that coating of CeO_2 with aSiO_2 substantially reduced CeO_2-induced acute lung inflammation and cytotoxicity at 24 h post-exposure (Demokritou et al., 2012).

The objective of the present study is to investigate further pulmonary responses to aSiO_2-coated CeO_2 (aSiO_2/CeO_2), CeO_2 and aSiO_2 nanoparticles in a time- and dose-dependent manner. The stability of aSiO_2 coating on CeO_2, and the development of pathological changes in CeO_2-, aSiO_2/CeO_2- and aSiO_2-exposed lungs were also evaluated.

2. Methods

2.1. Animals

Specific pathogen-free male Sprague–Dawley (Hla:SD-CVF) rats (6 weeks old, ~200 g) were purchased from Hilltop Laboratories (Scottdale, PA). Rats were kept in cages individually ventilated with HEPA-filtered air, housed in an Association for Assessment and Accreditation for Laboratory Animal Care (AAALAC)-approved facility, and provided food and water ad libitum. Animals were used after a 1 week acclimation period. All rats were exposed and euthanized according to a standardized experimental protocol that complied with the Guide for the Care and Use of Laboratory Animals and was approved by the institutional Animal Care and Use Committee.

2.2. Particle generation and characterization

CeO_2, aSiO_2/CeO_2 and aSiO_2 particles were generated using the VENGES and characterized as previously described (Demokritou et al., 2012). Briefly, X-ray diffraction (XRD) patterns were obtained using a Scintag XDS2000 powder diffractometer [Cu Kα (λ = 0.154 nm), −40 kV, 40 mA, stepsize = 0.02°]. The crystal size was determined by applying the Sherrer Shape Equation to the Gaussian fit of the major diffraction peak. The Brunauer–Emmett–Teller (BET) powder-specific surface area (SSA) of all samples was measured by nitrogen adsorption at 77 K (Micromeritics TriStar; Norcross, GA), after sample degassing for 1 h at 150 °C in nitrogen. BET equivalent primary particle size was calculated, under a spherical particle assumption, using $d_{BET} = 6000/(\rho \times SSA)$, where ρ is the material density. The zeta potential (ζ) and aggregate size of the particles dispersed in water (d_H) were measured using dynamic light scattering (DLS) with a Malvern Zetasizer Nano-ZS instrument (Malvern Instruments Ltd., Worcestershire, UK).

2.3. Exposure of animals

To prepare particle suspensions, CeO_2, aSiO_2/CeO_2, or aSiO_2 nanoparticles were suspended in sterile water (Mediatech, Inc.; Manassas, VA) and then sonicated for 1 min using an ultrasonic processor (Heat System-Ultrasonics; Plainview, NY). Particle suspensions were prepared immediately before usage and were vigorously vortexed to provide a well-mixed suspension immediately before each instillation, which occurred less than 1 min later.

For particle exposure, rats were anesthetized with sodium methohexital (35 mg/kg, i.p.) and placed on an inclined restraint board. At final concentrations of 0.15, 1 or 3.5 mg/kg body weight, which were defined as low, medium or high concentration in this paper. There were significant differences in the density of particles used in this study. The densities for CeO_2, aSiO_2/CeO_2 and aSiO_2 were 7.65, 5 and 2.65 g/cm³, respectively. In consideration of the different densities of the three particles, exposure doses of aSiO_2/CeO_2 and aSiO_2 were adjusted by density to the same particle number as for 0.15, 1 or 3.5 mg/kg body weight of CeO_2. Sterilized water was used to make nanoparticle suspensions and used as vehicle controls. The treated animals (at least six in each treatment group) were sacrificed at various time points post-exposure. The study design included different groups for the following sets of end points: inflammatory and acellular mediators; stability of aSiO_2 coating on the CeO_2 core; chemical analysis of particles in the digested lung tissues; and histological analysis of the lung tissues.

2.4. Isolation of AM and bronchoalveolar lavage fluid

Animals were injected with a lethal dose of euthanasia solution (sodium pentobarbital, 0.2 g/kg, i.p.) and exsanguinated by transecting the renal artery. AM were obtained by bronchoalveolar lavage (BAL) with a Ca^{2+}, Mg^{2+}-free phosphate-buffered medium (145 mM NaCl, 5 mM KCl, 1.9 mM NaH_2PO_4, 9.35 mM Na_2HPO_4, and 5.5 mM glucose; pH 7.4) as described previously (Yang et al., 2001). Briefly, the lungs were lavaged with 6 ml Ca^{2+}, Mg^{2+}-free phosphate-buffered medium in and out twice for the first lavage, and subsequently lavaged with 8 ml of the medium when ~80 ml BAL fluid (BALF) was collected from each rat. The acellular supernate from the first lavage was saved

separately from subsequent lavages for further analysis. Cell pellets from each animal were combined, washed, and resuspended in a HEPES-buffered medium (145 mM NaCl, 5 mM KCl, 10 mM HEPES, 5.5 mM glucose, and 1.0 mM $CaCl_2$; pH 7.4). Cell counts and purity were measured using an electronic cell counter equipped with a cell sizing attachment (Coulter model Multisizer II with a 256C channelizer; Beckman Coulter; Fullerton, CA).

2.5. Lactate dehydrogenase (LDH) activity and albumin content in first BALF and chemiluminescence (CL)

The LDH activity in the first acellular BALF was measured in fresh samples using Roche Diagnostic reagents and procedures (Roche Diagnostic Systems; Indianapolis, IN) on an automated Cobas C111 analyzer (Roche Diagnostic Systems). The albumin content in the first acellular BALF was measured based on albumin binding to bromcresol green with Roche Diagnostic reagents and procedures following the manufacturer's protocol.

Luminol-dependent CL, a measure of reactive oxygen species (ROS) formation, was monitored using a Berthold LB953 Luminometer (Berthold; Wildbad, Germany). CL generated by BAL cells (10^6 AM/ml) was measured before and after stimulation with unopsonized zymosan (2 mg/ml final concentration; Sigma-Aldrich; St. Louis, MO), a yeast cell wall that stimulates macrophages. The results were presented as total counts/15 min/10^6 AM. Zymosan-stimulated CL was calculated as the total counts in the presence of stimulant minus the corresponding basal counts as described by Yang et al. (2001) and Park et al. (2007).

2.6. Measurement of soluble mediators in the first acellular BALF and hydroxyproline content in the lung tissue

2.6.1. IL-12
IL-12 in first acellular BALF was determined using enzyme-linked immunosorbent assays (ELISA), obtained from Biosource International, Inc. (Camarillo, CA), according to the manufacturers' protocol.

2.6.2. MMP-2, MMP-9 and TIMP-1
The levels of MMP-2, MMP-9 and TIMP-1 were determined in the first acellular BAL fluid, using ELISA kits from Insight Genomics (Falls Church, VA), Cusabio Biotech Co., LTD. (Wuhan; Hubei, China), and R&D Systems Inc. (Minneapolis, MN), respectively, following the manufacturers' protocols.

2.6.3. Zymography
Zymography was used to study MMP activity. MMP activity was determined by the degradation of the substrate in the gel and identified by comparison to the molecular weight standard. To determine the MMP-9 activity in the first acellular BALF, 15 μg of acellullar BALF protein was loaded onto 10% Novex Zymogram (Gelatinase) gels, consisting of a 10% Tris-Glycine gel with 0.1% gelatin as the substrate (Life Technologies; Grand Island, NY), according to the manufacturer's instructions. Briefly, after electrophoresis, gels were incubated in renaturing buffer, washed with developing buffer, and incubated with developing buffer overnight for maximum sensitivity. The gels were then stained with Coomassie brilliant blue and destained in methanol-acetic acid-water until clear bands of enzymatic activity were at optimal contrast from the background. Molecular weight standards were run on each gel.

2.6.4. Hydroxyproline determination
The levels of collagen in the lungs were analyzed by measurement of hydroxyproline content in the lung tissues. Rat lungs were chopped and hydrolyzed in 6 N HCl for 48–72 h at 110 °C. Hydroxyproline was determined according to the method of Witschi et al. (1985).

2.7. Transmission electron microscope (TEM)

AM ultrastructure was analyzed by TEM. BAL cell pellets were fixed in Karnovsky's fixative (2.5% glutaraldehyde + 3% paraformaldehyde in 0.1 M sodium cacodylate, pH 7.4) and post-fixed with osmium tetroxide. Cells were dehydrated in graded alcohol solutions and propylene oxide and embedded in LX-112 (Ladd; Williston, VT). Ultrathin sections were stained with uranyl acetate and lead citrate and examined with a TEM (JEOL 122, Tokyo, Japan).

2.8. Elemental analysis by field emission scanning electron microscopy (SEM) energy dispersive X-ray spectroscopy (EDX)

For SEM analysis, lung tissues were fixed in formalin and post-fixed in osmium tetroxide. The samples were dehydrated in an ethanol series, dried using hexamethyldisilazane, mounted onto aluminum stubs and sputter-coated with gold/palladium. The samples were then imaged on a Hitachi S-4800 FESEM (Tokyo, Japan). The particles were then analyzed by a Bruker EDX (Berlin, Germany) for elemental analysis.

2.9. Digestion of lung tissue

Lung tissues from control and exposed animals were digested to obtain a concentrated particulate sample for better chemical analysis of the deposited particles by EDX. Lung tissue was digested according to the method reported by Ashoka et al. (2009) with minor modification. Briefly, 1.5 ml of concentrated nitric acid, 1 ml 30% hydrogen peroxide and 1.5 ml Milli-Q water were added to half of the lung in a 50 ml polypropylene tube. The cap was placed on loosely and the tube was placed inside a another container before placing it into a microwave oven (1300 W) and subjecting it to heating procedure, setting of power at 10% for 1 min and 30 s, and then allowed to cool for the same time period. The outer plastic container was used to prevent acid fumes from corroding the components of the microwave oven.

2.10. Histological examination and Sirius red staining for collagen detection

Rat lung tissues from different exposure groups were fixed immediately after sacrifice by IT of 10% neutral buffered formalin at a pressure of 30 cm H_2O (at an altitude of 960 ft), embedded in paraffin, and stained with hematoxylin and eosin for light microscopic examinations.

Collagen in the lungs was detected with Sirius red staining (Junqueira et al., 1979). Paraffin sections were deparaffinized and rehydrated with xylene-alcohol series to distilled water. The slides were then stained with 0.1% Picrosirius solution (100 mg of Sirius Red F3BA in 100 ml of saturated aqueous picric acid, pH 2), for 1–2 h, washed for 1 min in 0.01 N HCl, counterstained with Mayer's hematoxylin for 2 min, dehydrated, and mounted with a coverslip.

Morphometric measurement of AM and granulomatous tissue in the alveolar airspaces of Sirius red stained lung sections were determined. Point counting of AM (10 per section) taken at $40\times$ using a 120 point grid on a series of uniformly taken pictures of each section (2 sections per rat) was used. The points of either AM or granulomatous masses in the alveolar airspace were totaled and the result was expressed as a percentage of the alveolar region.

2.11. Statistical analysis

Data are presented as means ± standard errors. Comparisons were made using analysis of variance (ANOVA) with means testing by Dunnett's test to compare treatment groups to control or by Tukey–Kramer test to compare all groups. A $p \leq 0.05$ was considered to be significant.

Table 1
Characterization of CeO_2, $aSiO_2/CeO_2$ and $aSiO_2$.

Material	Theoretical		SSA		
	SiO_2 [wt.%]	$d_{XRD,core}$	[m^2/g]	d_H (nm)	ζ (mV)
$aSiO_2$	100	19 (d_{BET})	147	161	-28.4 ± 6.90
CeO_2	0	17.3	61	53 ± 4	37.8 ± 1.85
$aSiO_2/CeO_2$	20	21	50	131 ± 14	-38.4 ± 1.86

3. Results

3.1. ENM characterization

Previously-published TEM and SEM images of CeO_2, $aSiO_2/CeO_2$ and $aSiO_2$ samples collected in situ illustrate the fractal structure of the agglomerates formed by the flame synthesis method (Demokritou et al., 2012). Table 1 summarizes particle characterization data in powder form and dispersed in water. XRD-determined crystal size of uncoated CeO_2 (17.3 nm) was slightly smaller than that of SiO_2-coated CeO_2 (21 nm). The SSA of $aSiO_2$ was 147 m^2/g, corresponding to an equivalent diameter of 19 nm. The SSA of CeO_2 was 61 m^2/g and the SSA of $aSiO_2/CeO_2$ was 50 m^2/g, corresponding to an equivalent diameter of 12.8 nm and 19.2 nm, respectively. Differences between CeO_2 and $aSiO_2$-coated BET equivalent diameter are more pronounced than crystal sizes due to $aSiO_2$ encapsulation, which is not accounted for when measuring the crystal size.

Table 1 summarizes the hydrodynamic diameter (d_H) and zeta potential (ζ) of CeO_2, $aSiO_2/CeO_2$ or $aSiO_2$ dispersed in sterilized H_2O used for IT exposure. $aSiO_2/CeO_2$ and $aSiO_2$ exhibited similar agglomeration when dispersed in water. The negative zeta-potential measured for $aSiO_2/CeO_2$ and $aSiO_2$ dispersed in H_2O was significantly different from CeO_2 exhibited positive zeta potential.

3.2. Concentration and time dependent effects of $aSiO_2$ coating on CeO_2-induced lung inflammation and injury

Exposure of rats to CeO_2, $aSiO_2/CeO_2$ or $aSiO_2$ significantly induced lung inflammation (increased polymorphonuclear neutrophils, PMN), cytotoxicity (elevated LDH activity) and lung air/blood barrier damage (increased albumin) in a dose related manner 1 day after exposure, as shown in Fig. 1. The CeO_2- and $aSiO_2/CeO_2$-induced inflammation and cellular toxicity were sustained through 28 days post-exposure, though air/blood barrier damage was not sustained during this period. While partial recovery from $aSiO_2/CeO_2$-induced inflammation and cellular toxicity was observed, $aSiO_2$-induced acute lung inflammation and injury completely recovered at 28 days post-exposure. CeO_2, $aSiO_2/CeO_2$ and $aSiO_2$ activated AM production of ROS (CL) at 1 day post-exposure, but this activation was transient.

3.3. Effects of particle exposure on acellular mediator production

CeO_2, $aSiO_2/CeO_2$ and $aSiO_2$ induced IL-12 production and MMP-2 in the first acellular BALF at 1 day post-exposure (Fig. 2A, B), and this activation declined to the control level at 28 days after exposure. Exposure of rats to CeO_2 significantly increased MMP-9 (Fig. 2C) and TIMP-1 (Fig. 2D) levels in the first acellular BALF compared with the control at 1 day post-exposure, and returned to the control level at 28 days post-exposure. In contrast, $aSiO_2/CeO_2$ and $aSiO_2$ exposures induced MMP-9 level to a lesser extent that did not reach statistical significance. Also, $aSiO_2/CeO_2$ failed to significantly increase TIMP-1. Fig. 2E demonstrates that the MMP-9 activity in the first BALF was barely detectable in the control; however, it was substantially increased after CeO_2 exposure, but only slightly elevated after $aSiO_2/CeO_2$ or $aSiO_2$. Taken as a whole, the order of potency for enhancement of IL-12, MMP-2, MMP-9, and TIMP-1 levels as well as MMP-9 activity, was $CeO_2 \gg aSiO_2/CeO_2 \sim aSiO_2$.
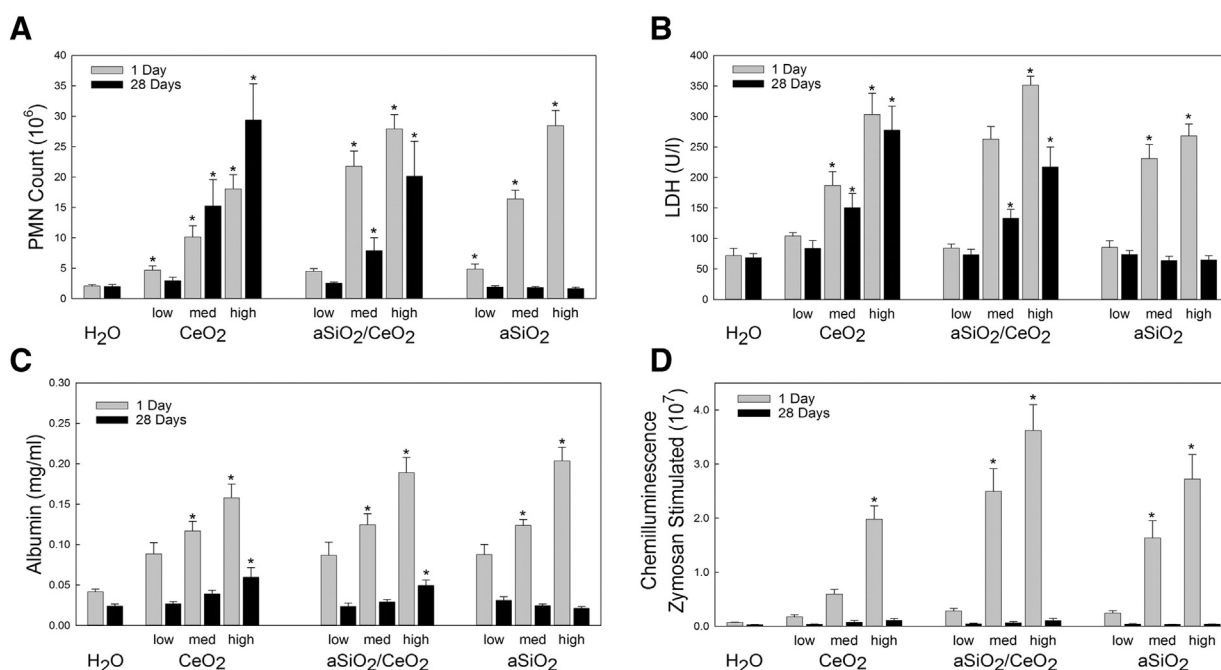

Fig. 1. Effects of CeO_2, $aSiO_2/CeO_2$ or $aSiO_2$ on lung inflammation, cytotoxicity, lung injury, and oxidant generation by AM. Effects of particle-induced PMN infiltration, a measure of lung inflammation (A); LDH activity in the first acellular lavage fluid, a marker for the cytotoxicity (B); the amount of albumin in the first acellular lavage fluid, an indicator for the leakage of air/capillary barrier (C); and CL generation by AM, a marker for oxidant generation (D). The samples were collected at 1 and 28 days post-exposure. *Significantly different from control; $p < 0.05$.
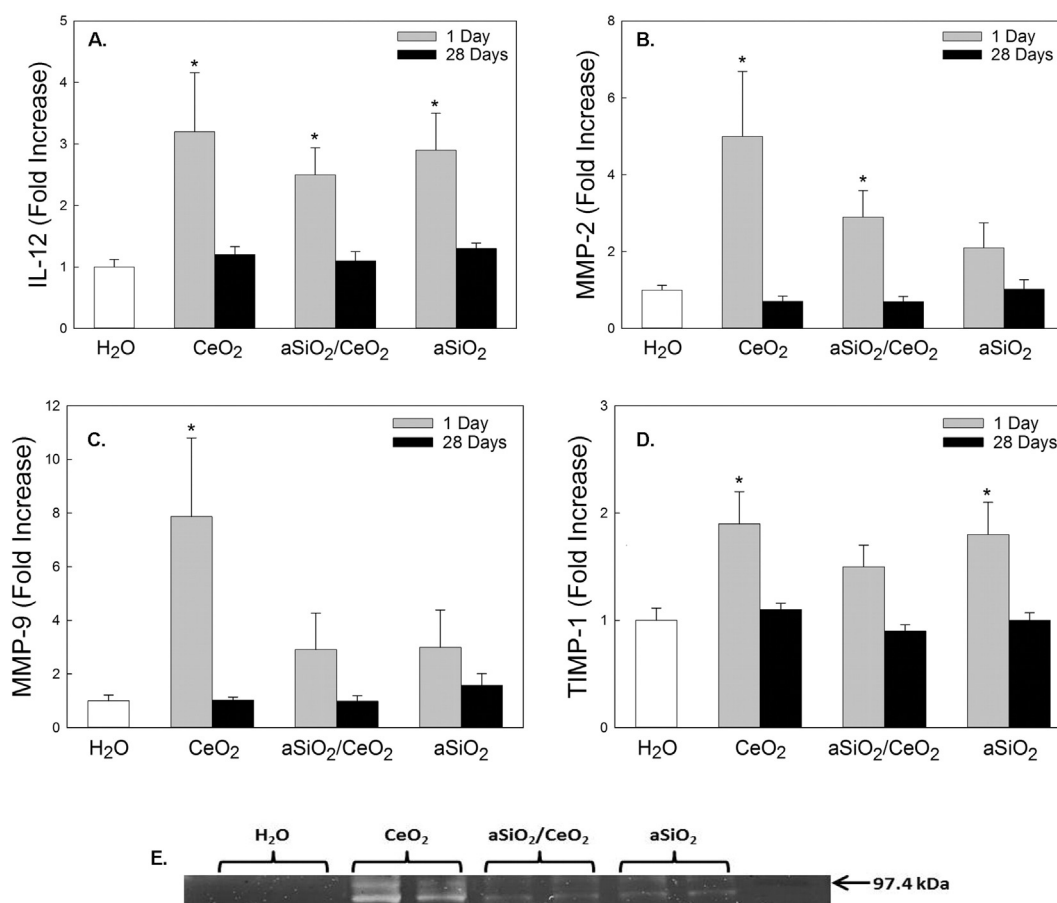
Fig. 2. Effects of particle exposure on IL-12, MMP-2, MMP-9 and TIMP-1 levels in the 1st BALF. The first acellular BALF was isolated from control and particle-exposed animals at 1- and 28-day post exposure. Time-dependent effects of particle induced inflammatory cytokine (A) and acellular mediators (B, C, and D) in the first acellular BALF, at 1 and 28 days post exposure, are shown. MMP-9 activity in the first acellular BALF from different treatment groups was monitored using Zymography at 1 day post exposure (E). *Significantly different from control; $p < 0.05$. The values are expressed as means $\pm$ SE, n = 6.

3.4. Pulmonary fibrosis

The development of lung fibrosis was determined via measurement of lung hydroxyproline, a specific marker for collagen, in particle-exposed lung tissues collected at 28 or 84 days post exposure. Fig. 3 shows that exposure of rats to the low dose of the particles did not significantly alter hydroxyproline level in the lung tissue up to 84 days post exposure. However, exposure of rats to middle and high doses of CeO_2, $aSiO_2/CeO_2$ or $aSiO_2$ significantly enhanced hydroxyproline content in the lung tissues at 28 and 84 days post-exposure when compared to the controls.

Morphometric analysis of the lung tissues to detect localized collagen formation via Sirius red staining showed that the low concentration of CeO_2, $aSiO_2/CeO_2$ and $aSiO_2$ did not induce lung fibrosis at 84 days after exposure (Fig. 4A). However, exposure of rats to the high concentration of CeO_2-, $aSiO_2/CeO_2$- or $aSiO_2$ induced lung fibrosis at 28 days after exposure (Fig. 4B). However, it appears qualitatively that the degree of fibrosis is greater after CeO_2 than $aSiO_2/CeO_2$ administration. Fig. 4B also shows that exposure of rats to the high dose of CeO_2 increased surfactant, AM and granulomatous tissues in alveolar airspace, when compared to $aSiO_2/CeO_2$- or $aSiO_2$-exposed rat lungs. Morphometric analysis of the lung tissue demonstrated that AM represents
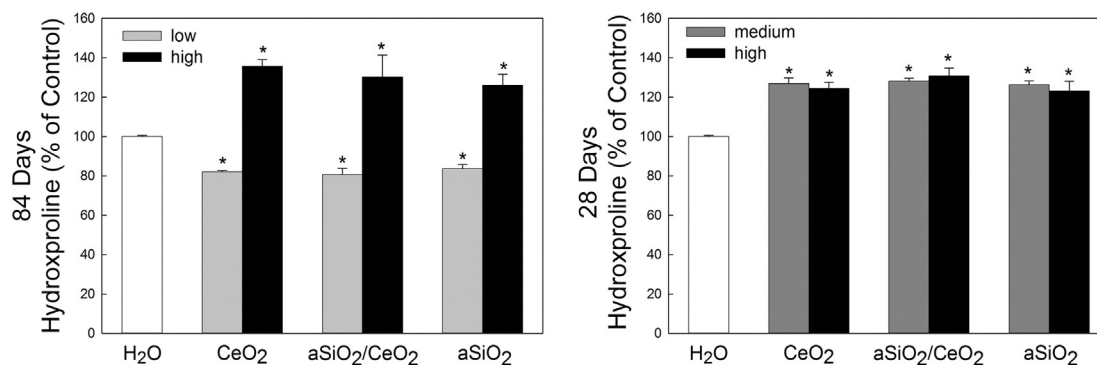

Fig. 3. Dose-dependent effects of CeO_2-, $aSiO_2/CeO_2$- and $aSiO_2$-induced lung hydroxyproline content in the lungs. Hydroxyproline content in the lung tissues of low- and high-dose particle-exposed animals at 84 days post exposure and medium- and high-dose particle-exposed animals at 28 days post exposure were monitored as described in the methods. The values are expressed as means $\pm$ SE, n = 6. *Significantly different from control; $p < 0.05$.
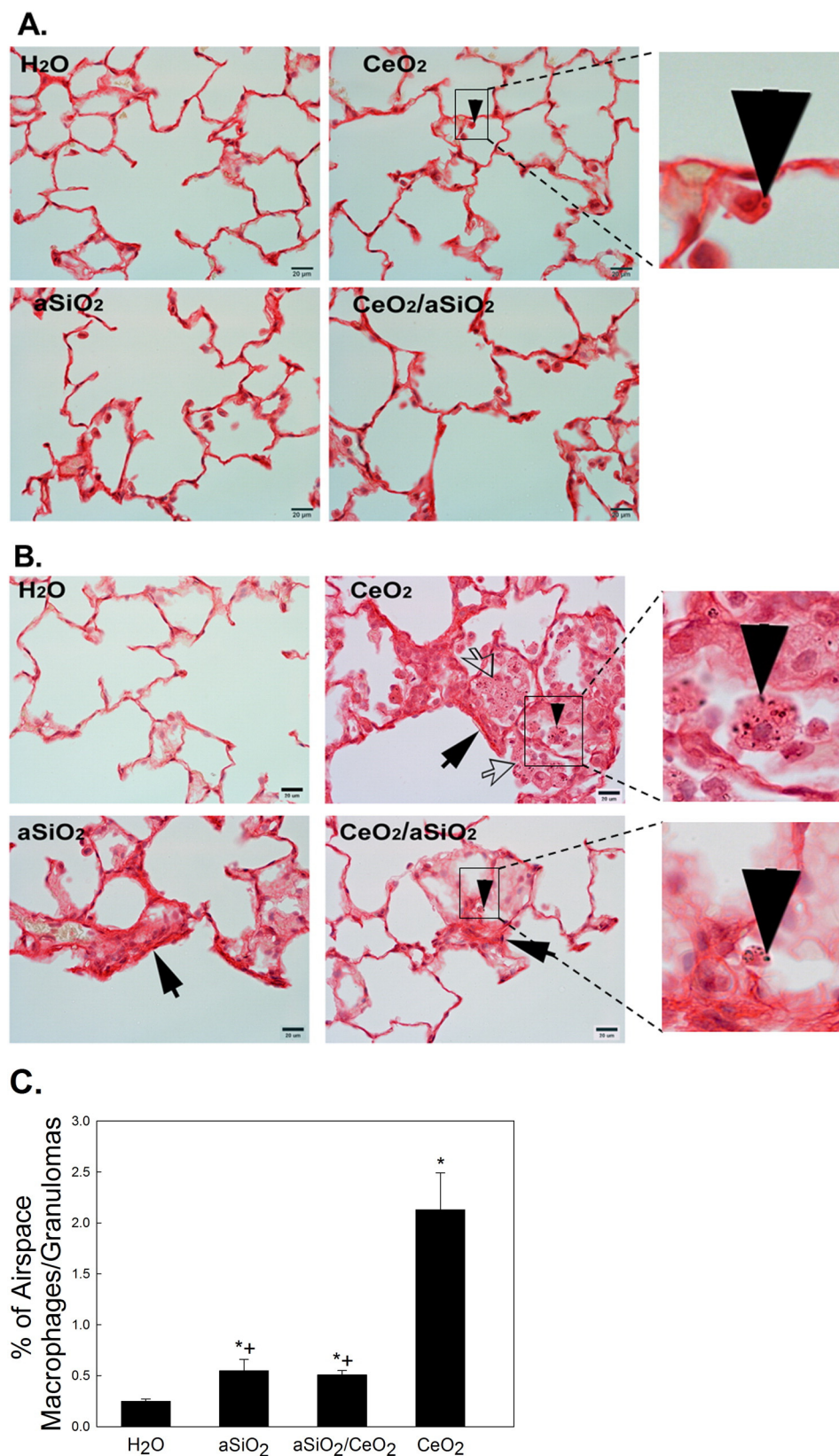
Fig. 4. Effects of CeO_2-, $aSiO_2/CeO_2$- and $aSiO_2$-exposure on Sirius Red staining for collagen formation in the lung tissue. Light micrograph of Sirius red staining for collagen formation in the lung tissues (arrow) at 84 days after low-dose exposure (A) and 28 days after high dose-exposure (B). The presence of particles in AM is indicated by the arrow head. Open arrows in the CeO_2 exposed lung indicate clusters of AM that are enlarged due to phagocytosis of alveolar surfactant debris. Panel C shows the percentage of alveolar macrophages and granulomatous tissue in the airspace of high dose CeO_2-exposed lungs at 28 days post exposure. *Significantly different from control; +significantly different from CeO_2-exposed lungs; $p < 0.05$. The values are expressed as means $\pm$ SE, n = 5.

0.25 percentage of the alveolar region of the control lung (Fig. 4 C), without granulomatous tissue in the lung. However, AM/granulomatous tissue of CeO_2-, $aSiO_2/CeO_2$-, and $aSiO_2$-exposed groups was significantly higher than the control, with that CeO_2- being 417% higher than the $aSiO_2/CeO_2$- and 387% higher than the $aSiO_2$-exposed lungs.

3.5. Presence of particles in the lung and elemental analysis of the particle

TEM micrographs revealed the presence of particles in all particle-exposed AM at 28 days post-exposure (Fig. 5). The results indicated that CeO_2 and $aSiO_2/CeO_2$ existed as solid particles, whereas $aSiO_2$ was amorphous in structure. However, EDX was not able to analyze the elements of the particles, which is probably due to the limited quantity of particles in the thin cuts of samples prepared for TEM analysis. Therefore, the thicker lung tissue samples were further analyzed by SEM for elemental analysis of the particles in the tissue.

SEM analysis showed particles in CeO_2- or $aSiO_2/CeO_2$-, but not $aSiO_2$-exposed lungs up to 28 days post-exposure. EDX analysis showed that Ce was a major element in lung tissue collected throughout the 28-day post CeO_2 (Fig. 6B, C, D, and E) or $aSiO_2/CeO_2$ exposures (Fig. 6G, H, I and J). Both Ce and Si were detected by EDX in $aSiO_2/CeO_2$-exposed lungs isolated at 1- and 3-day after exposure; however, only Ce but not Si was detected by EDX in $aSiO_2/CeO_2$-exposed lungs analyzed at 10- and 28-day after exposure. In comparison, Si was detected by EDX in $aSiO_2$-exposed lungs isolated at 1- and 3-day after exposure (Fig. 6L and M), but was not observed at 10- and 28-day post exposure (Fig. 6N and O). It is worth noting that phosphorus was detected by EDX in all particle-exposed lung tissues.

To confirm that $aSiO_2$ existed in the lung, all high dose particle-exposed lung tissues obtained at 28 days post exposure were digested in order to obtain more concentrated particle samples from the tissue. SEM and EDX on the digested lung tissue were monitored as shown in Fig. 7. The results indicate that Ce was present in CeO_2- and $aSiO_2/CeO_2$-exposed lungs at 28 days post-exposure.

However, while Si was detected 28 days after $aSiO_2$ exposure, it was not detected in $aSiO_2/CeO_2$-exposed lung tissues. This suggests that the $aSiO_2$ coating may dissolve off the particle with time in the lung.

4. Discussion

Recently, the wider use of cerium fuel borne catalyst in diesel engines has led to increased CeO_2 in the diesel exhaust and raises the potential long term health concerns (HEI, 2001). A "safer by design" concept to reduce CeO_2-induced toxicity was developed, which was based on the encapsulation of CeO_2 nanoparticles with a nanothin $aSiO_2$ layer (Gass et al., 2013). Based on this concept, studies were carried out in which CeO_2 particles with or without nanothin layer of $aSiO_2$ were generated and directly supplied to a whole body inhalation system. the results suggested that, in contrast to CeO_2 alone, $aSiO_2/CeO_2$ exposure did not induce acute pulmonary inflammation or lung damage at 1 day post exposure (Demokritou et al., 2012). This study provided valuable in vivo evidence that the $aSiO_2$-encapsulation could be protective in minimizing CeO_2-induced acute pulmonary inflammatory responses.

The present study demonstrated time- and dose effects of $aSiO_2$ coating on CeO_2-induced lung responses after IT exposure. The IT exposure was chosen for the present study due to the difficulty of the setting up the inhalation exposure, since particle generation system was located at Harvard, while rat exposure/response studies were conducted at NIOSH. The IT exposure method has been reported by an expert panel to be a useful method for screening the potential toxicity of a test material in the lower respiratory tract or for range finding of effective lung burdens (Driscoll et al., 2000). They also reported that particles delivered at <100 mg by IT appear to be cleared at a similar rate as would occur following inhalation of the same lung burden. Thus, this exposure procedure has been chosen for the present study. Exposure of rats to CeO_2, $aSiO_2/CeO_2$ or $aSiO_2$ markedly induced acute lung inflammation,
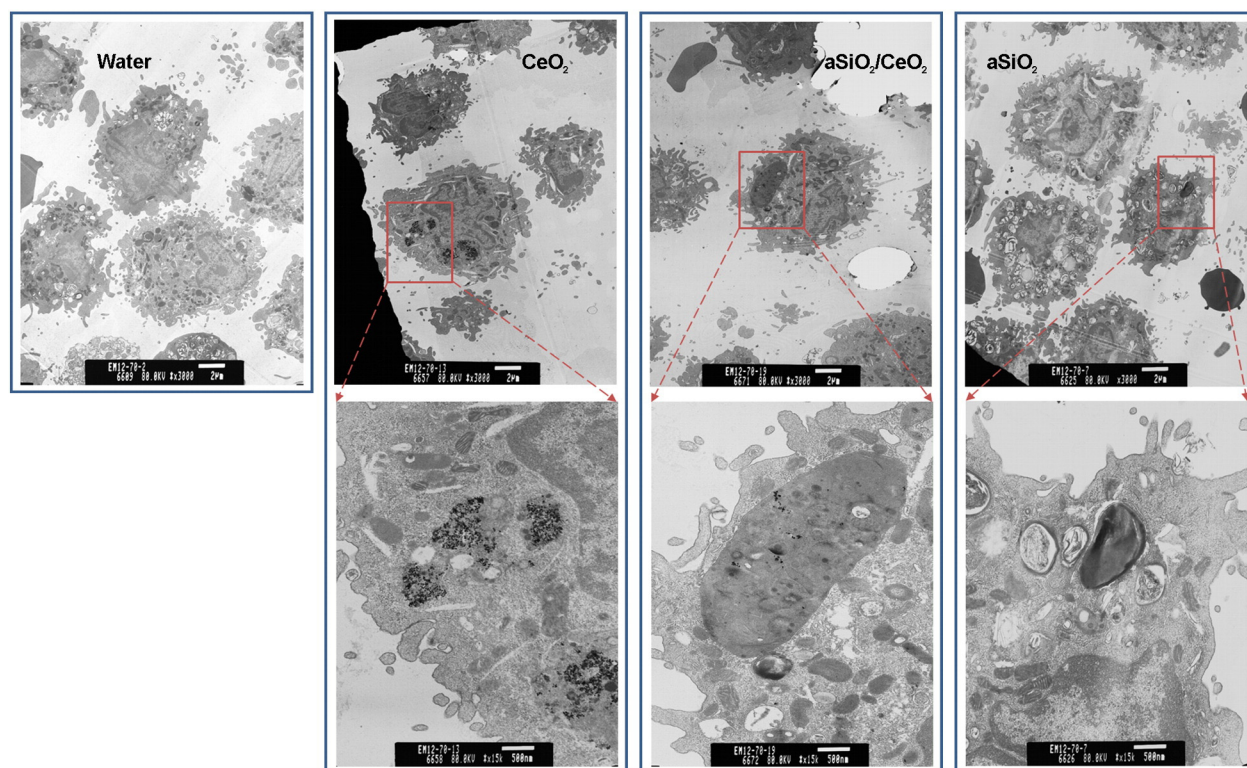

Fig. 5. TEM micrographs of particles in AM at 28 days post-exposure. AM were isolated by bronchoalveolar lavage from control, CeO_2-, $aSiO_2/CeO_2$-, and $aSiO_2$-exposed rats at 28 days post-exposure (scale bar = 2 μm in upper micrographs; scale bar = 500 nm in lower micrographs).
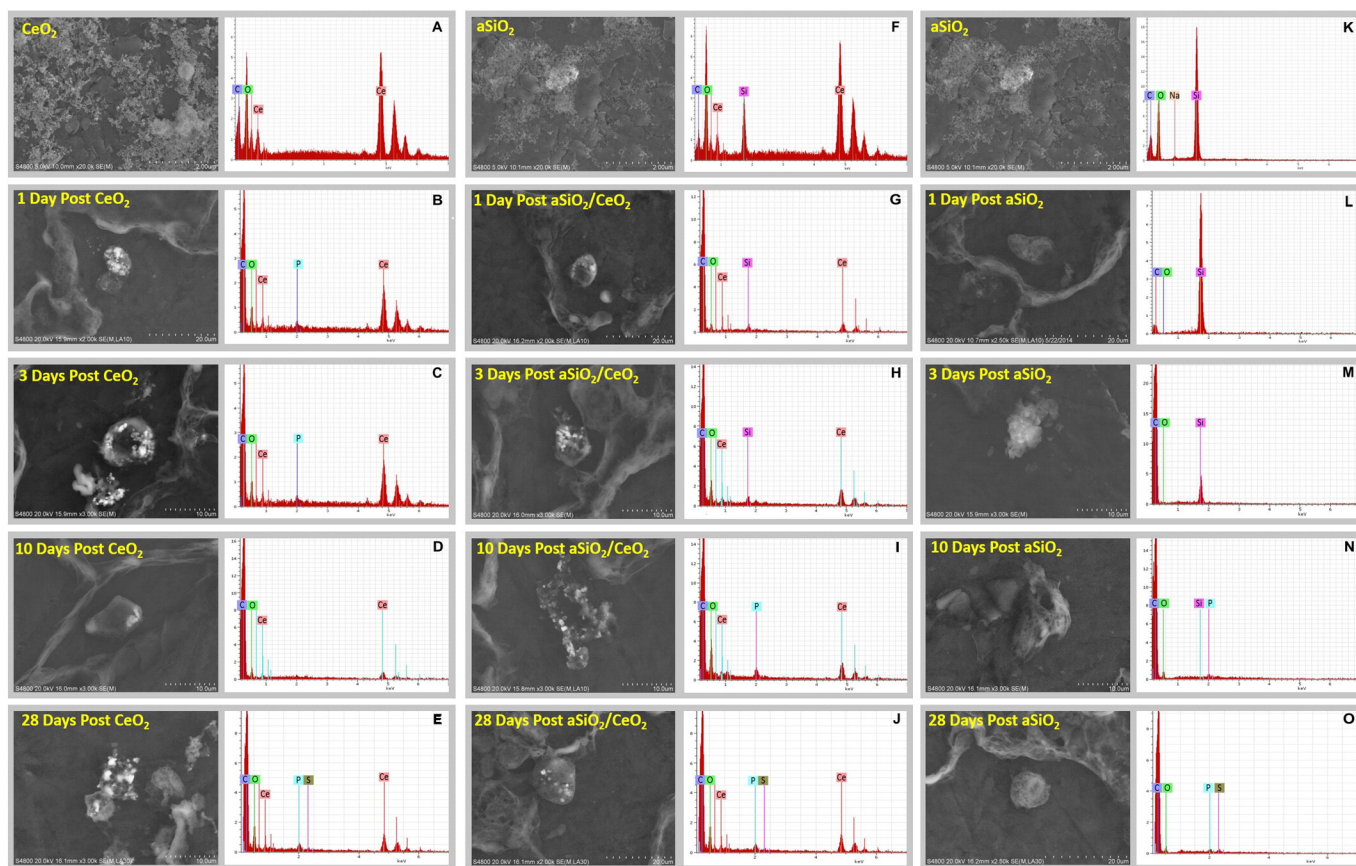
Fig. 6. SEM of particle-exposed lung tissues and qualitative chemical analysis of particles contained in the lung tissue. SEM of CeO$_2$, aSiO$_2$/CeO$_2$ and aSiO$_2$ raw particles are shown in the left side of panels of A, F and K, respectively. CeO$_2$, aSiO$_2$/CeO$_2$- and aSiO$_2$-exposed lungs collected at 1, 3, 10 and 28 days post exposure are shown. SEM of particle-exposed lung tissue was presented on the right side of each panel. Qualitative chemical analysis with spatial resolution of 10 nm using EDX was performed and presented in the right side of each panel, alongside the SEM.

cytotoxicity and air/capillary injury in a dose-dependent manner at 1 day post exposure (Fig. 1). It is worth noting that CeO$_2$-induced acute inflammation and cellular injury were persistent through a 28 day-exposure time period, which is in agreement with our previous findings that exposure of rats to commercially available CeO$_2$ induced persistent pulmonary inflammation (Ma et al., 2011). aSiO$_2$/CeO$_2$ exposure induced inflammation and cytotoxicity were partially attenuated when monitored at 28 days post-exposure, the thin coating appeared lower CeO$_2$-induced inflammation but did not reach statistical difference. The aSiO$_2$ elicited pulmonary inflammation; however, the response was transient, which is in agreement with previously reported findings (Chen et al., 2004; Cho et al., 2007; Merget et al., 2002). In addition, Warheit et al. (1995) have demonstrated that exposure of rats to short-term inhalation of amorphous silica produced a transient pulmonary inflammatory response.

All particles significantly activated ROS generation in AM at 1 day after exposure (Fig. 1). This activation of AM returned to the control level at 28 days post-exposure. Since aSiO$_2$ exposure alone stimulated AM ROS generation, it is not surprising that the aSiO$_2$ thin coating did not protect AM from activating ROS production.

It is known that the balance between ECM synthesis and degradation of matrix components is crucial for tissue repair. To preserve such a balance, MMPs, which represent a family of extracellular and cell surface-associated proteinases, and their physiological inhibitors, TIMPs, are both involved to assure normal lung development and proper wound healing. Abnormal activation of proteolytic and/or antiproteolytic functions can lead to lung diseases, including fibrosis (Gueders et al., 2006). Our previous study demonstrated that CeO$_2$ exposure induced

MMP/TIMP imbalance, which may have played a role in the reported collagen formation in the lung (Ma et al., 2012). The present study demonstrates that all particles induced the production of pro-inflammatory cytokine, IL-12 (Fig. 2). CeO$_2$ increased ECM collagen degradation enzyme MMP-2 and MMP-9 levels, whereas CeO$_2$ and aSiO$_2$ increased TIMP-1 level in the acellular BALF. In general, aSiO$_2$/CeO$_2$ was less effective in stimulating such responses. Our study also established that CeO$_2$ increased MMP-9 activity to a much higher extent than aSiO$_2$/CeO$_2$. These differential effects of CeO$_2$ and aSiO$_2$/CeO$_2$ particles on ECM balance suggest that mechanisms involved in ECM degradation and regeneration may be altered. It is known that the in vivo activity of MMPs is under tight control, and MMPs are generally expressed in very low amounts, while the concentration of TIMP can far exceed MMPs in tissue and extracellular fluids in order to limit their proteolytic activity to focal pericellular sites. The elevated MMP-2 and MMP-9 production may play a role in basement membrane disruption and enhancement of fibroblast invasion to the alveolar spaces. The results from the present study showed that TIMP-1/MMP-9 ratio was reduced from 460 (control) to 110 (CeO$_2$-exposed lungs) or 243 (aSiO$_2$/CeO$_2$-exposed lungs). These results demonstrate over-production of MMP-9 with significantly increased activity that may play an important role in ECM remodeling and development of fibrosis. Increased levels of MMP-2 and MMP-9 in epithelial lining fluid, which have been implicated in the development of fibrosis, were also observed in IPF patients (Lemjabbar et al., 1999). Therefore, the results support the hypothesis that aSiO$_2$ coating of CeO$_2$ may limit the fibrotic response.

The present study showed that medium and high doses of all particles resulted in an increase in the lung content of hydroxyproline,
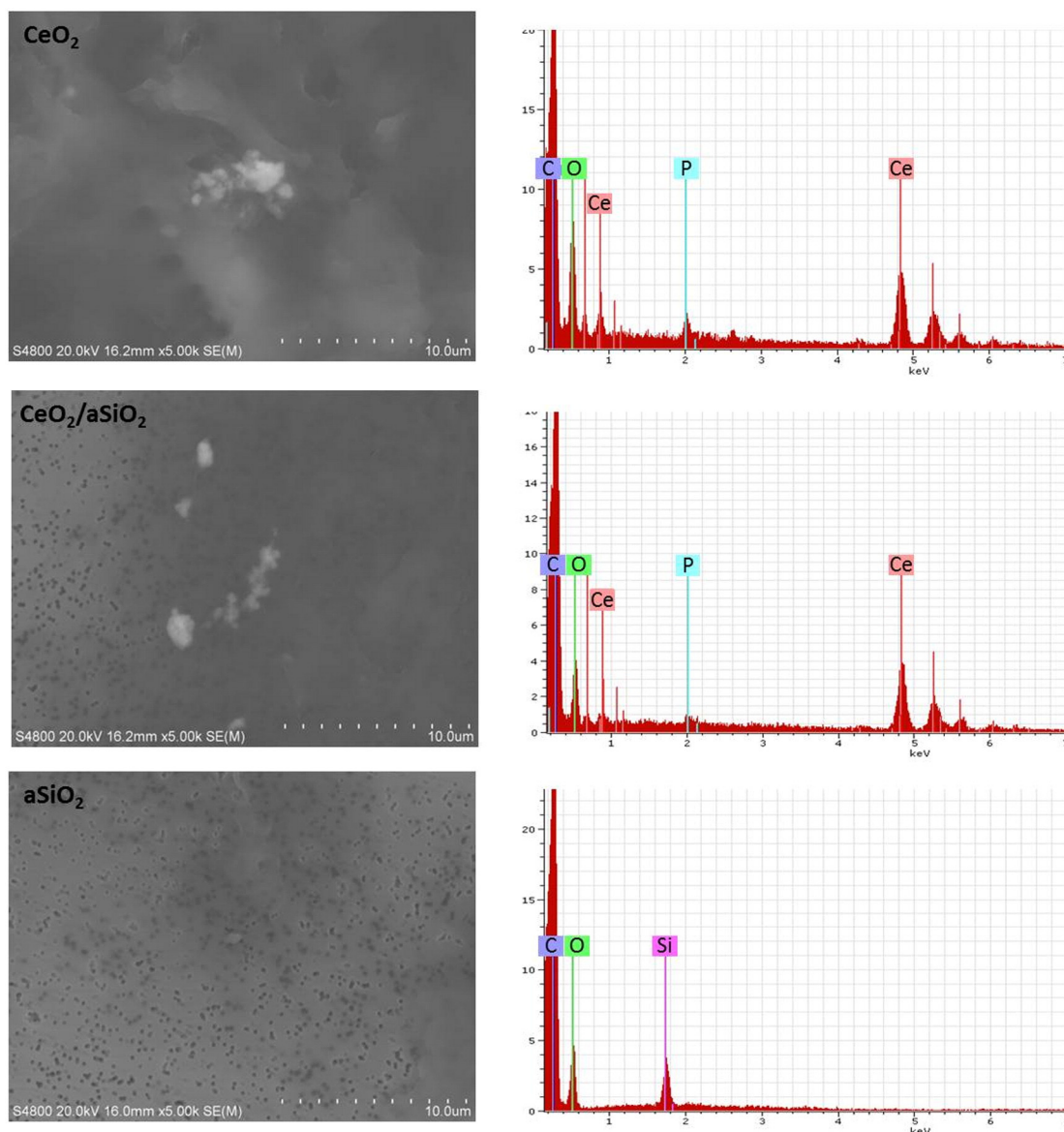
Fig. 7. SEM EDX of digested lungs. Particle-exposed lungs collected at 28 days post-exposure were digested with nitric acid and hydrogen peroxide to obtain the particles retained in the exposed lungs. SEM micrographs of CeO_2-, $aSiO_2/CeO_2$- and $aSiO_2$-digested lungs and EDX of the elemental analysis of the particles in the lungs are shown.

which is a marker for pulmonary fibrosis (Fig. 3). The dose- and time-dependent increase in hydroxyproline further illustrates this fibrotic process. Exposure of rats to the low dose of CeO_2, $aSiO_2/CeO_2$ or $aSiO_2$ did increase hydroxyproline or collagen deposition in the lungs even at 84 days post-exposure (Fig. 3). At high dose of CeO_2 particles, Sirius red staining of lung tissues for localized collagen formation confirmed substantial interstitial fibrosis in the lung tissues at 28 days post-exposure. The degree of Sirius red stained collagen was substantially lower at 28 day after a high dose exposure to $aSiO_2/CeO_2$ (Fig. 4B). These results suggest that $aSiO_2$ coating on CeO_2 was somewhat protective against the development of interstitial fibrosis.

Histopathological analyses showed severe phospholipidosis in CeO_2-exposed lungs, whereas only minimum accumulation of surfactant was found in $aSiO_2/CeO_2$- and $aSiO_2$-exposed lungs at 28 days post exposure. Phospholipidosis has been reported as an important feature in the CeO_2-induced fibrosis (Ma et al., 2011). The substantially reduced phospholipidosis after exposure to $aSiO_2$ coated CeO_2 particles would correlate with an alternation in the fibrogenic responses. The significant reduction of CeO_2-induced airspace AM and granulomatous

response in $aSiO_2/CeO_2$- exposed lungs (Fig. 4C), suggest that $aSiO_2$ coating substantially protect CeO_2-induced inflammatory responses.

Occupational exposure to RE metals, such as cerium has been shown to induce rare earth pneumoconiosis. Several RE pneumoconiosis cases have been reported (McDonald et al., 1995; Sabbioni et al., 1982), indicating that particles deposited in the lungs of workers exposed to RE-containing fumes result in severe pulmonary fibrosis. Ce was reported as major element in these lungs. Clearance of Ce from the deep lung appeared to be slow. Some significant Ce levels were found in the lung of patients 20 years after they stopped exposure to cerium (Pairon et al., 1995). The presence of CeO_2 particles in CeO_2-exposed rats has been demonstrated in our previous studies (Ma et al., 2011, 2012, 2014). The presence of CeO_2 and $aSiO_2/CeO_2$ particles in the AM of the CeO_2 or $aSiO_2/CeO_2$-exposed lung tissues up to 28 days post-exposure were demonstrated in TEM micrographs (Fig. 5). In contrast, $aSiO_2$ appeared as gel like substance in the $aSiO_2$-exposed lungs due to the amorphous characteristic of this particle. We examined the fate of $aSiO_2$ coating on CeO_2 in exposed rat lungs using SEM with the EDX spectrum analysis. The results clearly indicate that Ce was present in CeO_2- or $aSiO_2$/

CeO$_2$-exposed lungs through the 28 day post-exposure time period (Figs. 6, 7). In the aSiO$_2$/CeO$_2$-exposed lungs, EDX analysis revealed Si in the lung tissue collected at 1- and 3-day, but not at 10- and 28-day post-exposure (Fig. 6). These findings suggest that there may be dissolution of the aSiO$_2$ coating from CeO$_2$ particles with time in the lungs. In aSiO$_2$-exposed lungs, Si was not observed by EDX analysis at any exposure time point through 28-day post-exposure period (Fig. 6). However, the presence of Si in aSiO$_2$-exposed lungs was demonstrated in digested tissue (Fig. 7). EDX spectra of digested lung tissue demonstrated Ce in both CeO$_2$- and aSiO$_2$/CeO$_2$-exposed lungs, but did not reveal Si in aSiO$_2$/CeO$_2$-exposed lungs at 28 days post exposure, which supports the view that there is dissolution of the aSiO$_2$ coating. McDonald et al. (1995) have demonstrated, using SEM with EDX analysis, numerous particles deposited in the lung of a rare earth pneumoconiosis patient who was exposed to CeO$_2$ in the occupational setting of optical lens manufacturing. It is well known that EDX is used for qualitative analysis, rather than quantitative determinations of the specific elements present in samples. In the present study we used EDX analysis to demonstrate the elemental content of the deposited particles in the particle-exposed lungs, which provided useful information. However, to provide quantitative information of time-dependent dissolution of aSiO$_2$ coating would require more detailed and reliable methods, such as isotope tracing or inductively coupled plasma mass spectroscopy. In addition to the Ce and Si found in the exposed lung tissues, SEM and EDX analysis found that elemental phosphorus, P, was also present in all exposed lungs. In the CeO$_2$- and aSiO$_2$/CeO$_2$-exposed lungs the Ce to P ratio was much higher than one, suggesting that a small amount of Ce particles may be transformed by acid phosphatase in lysosomes to CePO$_4$, while most Ce remained in the crystalline structure. In the aSiO$_2$-exposed lung tissues, EDX also showed the presence of a small amount of P, suggesting that some of aSiO$_2$ was also transformed by lysosomal phosphatase. Evidence supporting transformation of insoluble particles in AM has been reported by Berry et al. (1997) using microanalysis, detecting amorphous deposits after inhalation of CeO$_2$ containing high concentrations of phosphorus associated with Ce, as insoluble CePO$_4$, in AM lysosomes.

In summary, the present study shows that CeO$_2$ induced sustained lung inflammation and cytotoxicity, as well as an acute imbalance of MMPs and TIMP-1 that favors fibrogenesis. Indeed, CeO$_2$ exposure substantially increased interstitial collagen level was correlated with the persistent presence of CeO$_2$ in the exposed lung tissue, as demonstrated by EDX analysis. A thin coating of aSiO$_2$ on CeO$_2$ reduced CeO$_2$ induced inflammatory response, decreased TIMP-MMP-9 ratio, reduced the accumulation of surfactant in the air space, and reduced CeO$_2$-induced interstitial collagen development. Therefore, the present study supports the "safer by design" concept of encapsulation of CeO$_2$ with a nanothin layer of aSiO$_2$ during their synthesis to partially protect against CeO$_2$-induced pulmonary responses, even though measurable dissolution of the coating from the CeO$_2$ particles occurred. Such a concept may be used for coating other flame generated nanoparticles to mitigate some of the occupational and environmental health concerns.

Conflict of interest

This research was partially supported with an NSF grant (#1235806) and NIEHS grant (#ES 0000002) for Dr. Joel M. Cohen and Dr. Philip Demokritou. There are no other competing interests.

Disclaimer

The findings and conclusions in this report have not been formally disseminated by the NIOSH and should not be construed to represent any agency determination or policy. Mention of brand name does not constitute product endorsement.

References

Ashoka, S., Peake, B.M., Bremner, G., Hageman, K.J., Reid, M.R., 2009. Comparison of digestion methods for ICP-MS determination of trace elements in fish tissues. Anal. Chim. Acta 653, 191–199.

Berry, J.P., Zhang, L., Galle, P., Ansoborlo, E., Henge-Napoli, M.H., Donnadieu-Claraz, M., 1997. Role of alveolar macrophage lysosomes in metal detoxification. Microsc. Res. Tech. 36, 313–323.

Cassee, F.R., Campbell, A., Boere, A.J., McLean, S.G., Duffin, R., Krystek, P., et al., 2012. The biological effects of subacute inhalation of diesel exhaust following addition of cerium oxide nanoparticles in atherosclerosis-prone mice. Environ. Res. 115, 1–10.

Chen, Y., Chen, J., Dong, J., Jin, Y., 2004. Comparing study of the effect of nanosized silicon dioxide and microsized silicon dioxide on fibrogenesis in rats. Toxicol. Ind. Health 20, 21–27.

Cho, W.S., Choi, M., Han, B.S., Cho, M., Oh, J., Park, K., et al., 2007. Inflammatory mediators induced by intratracheal instillation of ultrafine amorphous silica particles. Toxicol. Lett. 175, 24–33.

Cohen, J.M., Derk, R., Wang, L., Godleski, J., Kobzik, L., Brain, J., Demokritou, P., 2014. Tracking translocation of industrially relevant engineered nanomaterials (ENMs) across alveolar epithelial monolayers in vitro. Nanotoxicology. http://dx.doi.org/10.3109/17435390.2013.879612.

Demokritou, P., Gass, S., Pyrgiotakis, G., Cohen, J.M., Goldsmith, W., McKinney, W., et al., 2012. An in vivo and in vitro toxicological characterization of realistic nanoscale CeO2 inhalation exposures. Nanotoxicology 7, 1338–1350.

Driscoll, K.E., Costa, D.L., Hatch, G., Henderson, R., Oberdorster, G., Salem, H., Schlesinger, R.B., 2000. Intratracheal instillation as an exposure technique for the evaluation of respiratory tract toxicity: uses and limitations. Toxicol. Sci. 55, 24–35 (Review, 57 refs).

Fischer, H.C., Chan, W.C., 2007. Nanotoxicity: the growing need for in vivo study. Curr Opin Biotechnol 18, 565–571.

Gass, S., Cohen, J.M., Pyrgiotakis, G., Sotiriou, G.A., Pratsinis, S.E., Demokritou, P., 2013. A safer formulation concept for flame-generated engineered nanomaterials. ACS Sustain. Chem. Eng. 1, 843–857.

Gueders, M.M., Foidart, J.M., Noel, A., Cataldo, D.D., 2006. Matrix metalloproteinases (MMPs) and tissue inhibitors of MMPs in the respiratory tract: potential implications in asthma and other lung diseases. Eur. J. Pharmacol. 533, 133–144.

He, X., Zhang, H., Ma, Y., Bai, W., Zhang, Z., Lu, K., et al., 2010. Lung deposition and extrapulmonary translocation of nano-ceria after intratracheal instillation. Nanotechnology 21, 285103.

Health Effects Institute (HEI), 2001. In: Hibbs Jr., J.B. (Ed.), Evaluation of Human Health Risk from Cerium added to Diesel Fuel. HEI Communication, Boston, MA, USA, p. 9.

Junqueira, L.C., Bignolas, G., Brentani, R.R., 1979. Picrosirius staining plus polarization microscopy, a specific method for collagen detection in tissue sections. Histochem. J. 11, 447–455.

Lemjabbar, H., Gosset, P., Lechapt-Zalcman, E., Franco-Montoya, M.L., Wallaert, B., Harf, A., et al., 1999. Overexpression of alveolar macrophage gelatinase B (MMP-9) in patients with idiopathic pulmonary fibrosis: effects of steroid and immunosuppressive treatment. Am. J. Respir. Cell Mol. Biol. 20, 903–913.

Ma, J.Y., Zhao, H., Mercer, R.R., Barger, M., Rao, M., Meighan, T., et al., 2011. Cerium oxide nanoparticle-induced pulmonary inflammation and alveolar macrophage functional change in rats. Nanotoxicology 5, 312–325.

Ma, J.Y., Mercer, R.R., Barger, M., Schwegler-Berry, D., Scabilloni, J., Ma, J.K., et al., 2012. Induction of pulmonary fibrosis by cerium oxide nanoparticles. Toxicol. Appl. Pharmacol. 262, 255–264.

Ma, J.Y., Young, S.H., Mercer, R.R., Barger, M., Schwegler-Berry, D., Ma, J.K., et al., 2014. Interactive effects of cerium oxide and diesel exhaust nanoparticles on inducing pulmonary fibrosis. Toxicol. Appl. Pharmacol. 278, 135–147.

McDonald, J.W., Ghio, A.J., Sheehan, C.E., Bernhardt, P.F., Roggli, V.L., 1995. Rare earth (cerium oxide) pneumoconiosis: analytical scanning electron microscopy and literature review. Mod. Pathol. 8, 859–865.

Merget, R., Bauer, T., Kupper, H.U., Philippou, S., Bauer, H.D., Breitstadt, R., et al., 2002. Health hazards due to the inhalation of amorphous silica. Arch. Toxicol. 75, 625–634.

Molina, R., Konduru, N., Jimenez, R., Pyrgiotakis, G., Demokritou, P., Wohlleben, W., Brain, J., 2014. Bioavailability, distribution and clearance of tracheally instilled, gavaged or injected cerium dioxide nanoparticles and ionic cerium. Environ. Sci. Nano 1, 561–573.

Nalabotu, S.K., Kolli, M.B., Triest, W.E., Ma, J.Y., Manne, N.D., Katta, A., et al., 2011. Intratracheal instillation of cerium oxide nanoparticles induces hepatic toxicity in male Sprague–Dawley rats. Int. J. Nanomedicine 6, 2327–2335.

Pairon, J.C., Roos, F., Sebastien, P., Chamak, B., bd-Alsamad, I., Bernaudin, J.F., et al., 1995. Biopersistence of cerium in the human respiratory tract and ultrastructural findings. Am. J. Ind. Med. 27, 349–358.

Park, B., Martin, P., Harris, C., Guest, R., Whittingham, A., Jenkinson, P., et al., 2007. Initial in vitro screening approach to investigate the potential health and environmental hazards of Envirox™ — a nanoparticulate cerium oxide diesel fuel additive. Part. Fibre Toxicol. 4, 12.

Park, E.J., Cho, W.S., Jeong, J., Yi, J.H., Choi, K., Kim, Y., 2010. Induction of inflammatory responses in mice treated with cerium oxide nanoparticles by intratracheal instillation. J. Health Sci. 56, 387–396.

Porru, S., Placidi, D., Quarta, C., Sabbioni, E., Pietra, R., Fortaner, S., 2001. The potential role of rare earths in the pathogenesis of interstitial lung disease: a case report of movie projectionist as investigated by neutron activation analysis. J. Trace Elem. Med. Biol. 14, 232–236.

Prospect, 2009. Toxicological review of nano cerium oxide. Support of Prospect: Ecotoxicology Test Protocols for representative Nanomaterials in Support of the OECD Sponsorship Programme. http://www.nanotechia-prospect.org/managed_assets/ files/ prospect_nano_ceo2_literature_review.pdf.

Sabbioni, E., Pietra, R., Gaglione, P., Vocaturo, G., Colombo, F., Zanoni, M., et al., 1982. Long-term occupational risk of rare-earth pneumoconiosis. A case report as investigated by neutron activation analysis. Sci. Total Environ. 26, 19–32.

Schmoll, L.H., Elzey, S., Grassian, V.H., O'Shaughnessy, P.T., 2009. Nanoparticle aerosol generation methods from bulk powders for inhalation exposure studies. Nanotoxicology 3, 265–275.

Selman, M., Ruiz, V., Cabrera, S., Segura, L., Ramirez, R., Barrios, R., et al., 2000. TIMP-1, -2, -3, and -4 in idiopathic pulmonary fibrosis. A prevailing nondegradative lung microenvironment? Am. J. Physiol. Lung Cell. Mol. Physiol. 279, L562–L574.

Semmler-Behnke, M., Takenaka, S., Fertsch, S., Wenk, A., Seitz, J., Mayer, P., et al., 2007. Efficient elimination of inhaled nanoparticles from the alveolar region: evidence for interstitial uptake and subsequent reentrainment onto airways epithelium. Environ. Health Perspect. 115, 728–733.

Snow, S.J., McGee, J., Miller, D.B., Bass, V., Schladweiler, M.C., Thomas, R.F., et al., 2014. Inhaled diesel emissions generated with cerium oxide nanoparticle fuel additive induce adverse pulmonary and systemic effects. Toxicol. Sci. 142, 403–417.

Srinivas, A., Rao, P.J., Selvam, G., Murthy, P.B., Reddy, P.N., 2011. Acute inhalation toxicity of cerium oxide nanoparticles in rats. Toxicol. Lett. 205, 105–115.

Toya, T., Takata, A., Otaki, N., Takaya, M., Serita, F., Yoshida, K., et al., 2010. Pulmonary toxicity induced by intratracheal instillation of coarse and fine particles of cerium dioxide in male rats. Ind. Health 48, 3–11.

Warheit, D.B., McHugh, T.A., Hartsky, M.A., 1995. Differential pulmonary responses in rats inhaling crystalline, colloidal or amorphous silica dusts. Scand. J. Work Environ. Health 21 (Suppl. 2), 19–21.

Witschi, H.P., Tryka, A.F., Lindenschmidt, R.C., 1985. The many faces of an increase in lung collagen. Fundam. Appl. Toxicol. 5, 240–250.

Yang, H.M., Antonini, J.M., Barger, M.W., Butterworth, L., Roberts, B.R., Ma, J.K., et al., 2001. Diesel exhaust particles suppress macrophage function and slow the pulmonary clearance of Listeria monocytogenes in rats. Environ. Health Perspect. 109, 515–521.